





MICU1 occludes the mitochondrial calcium uniporter in divalent-free conditions

Macarena Rodríguez-Prados^{a,1} , Elena Berezhnaya^{a,1} , Maria Teresa Castromonte^a, Sergio L. Menezes-Filho^a, Melanie Paillard^a, and György Hajnóczky^{a,2}

Edited by Richard Lewis, Stanford University, Stanford, CA; received November 6, 2022; accepted March 30, 2023

Mitochondrial Ca^{2+} uptake is mediated by the mitochondrial uniporter complex (mtCU) that includes a tetramer of the pore-forming subunit, MCU, a scaffold protein, EMRE, and the EF-hand regulatory subunit, MICU1 either homodimerized or heterodimerized with MICU2/3. MICU1 has been proposed to regulate Ca^{2+} uptake via the mtCU by physically occluding the pore and preventing Ca^{2+} flux at resting cytoplasmic $[\text{Ca}^{2+}]$ (free calcium concentration) and to increase Ca^{2+} flux at high $[\text{Ca}^{2+}]$ due to cooperative activation of MICUs EF-hands. However, mtCU and MICU1 functioning when its EF-hands are unoccupied by Ca^{2+} is poorly studied due to technical limitations. To overcome this barrier, we have studied the mtCU in divalent-free conditions by assessing the Ru265-sensitive Na^+ influx using fluorescence-based measurement of mitochondrial matrix $[\text{Na}^+]$ (free sodium concentration) rise and the ensuing depolarization and swelling. We show an increase in all these measures of Na^+ uptake in MICU1KO cells as compared to wild-type (WT) and rescued MICU1KO HEK cells. However, mitochondria in WT cells and MICU1 stable-rescued cells still allowed some Ru265-sensitive Na^+ influx that was prevented by MICU1 in excess upon acute overexpression. Thus, MICU1 restricts the cation flux across the mtCU in the absence of Ca^{2+} , but even in cells with high endogenous MICU1 expression such as HEK, some mtCU seem to lack MICU1-dependent gating. We also show rearrangement of the mtCU and altered number of functional channels in MICU1KO and different rescues, and loss of MICU1 during mitoplast preparation, that together might have obscured the pore-blocking function of MICU1 in divalent-free conditions in previous studies.

mitochondrial calcium uniporter | MICU1 | Na^+ | EMRE | mitoplast

Ca^{2+} entry into mitochondria regulates cellular bioenergetics and survival and shapes intracellular Ca^{2+} signals (1–3). Mitochondrial Ca^{2+} uptake is mediated by the mitochondrial uniporter complex (mtCU) that includes a tetramer of the pore-forming subunit, mitochondrial calcium uniporter (MCU) (4, 5), and scaffold protein, essential MCU regulator (EMRE) (6), with the regulatory subunit, mitochondrial calcium uptake 1 (MICU1) (7) either homodimerized or heterodimerized with MICU2 (8) or MICU3 (9–16). MICUs have a pair of EF-hands that allows them to regulate Ca^{2+} uptake via mtCU in a Ca^{2+} -dependent fashion (7). MICU1 and MICU2 EF-hand mutants were reported to completely abolish mitochondrial Ca^{2+} uptake (17). MICU1 absence leads to the loss of Ca^{2+} dependence of mitochondrial Ca^{2+} uptake that was first observed as an increased Ca^{2+} uptake via mtCU at low $[\text{Ca}^{2+}]$ (free calcium concentration) and decreased Ca^{2+} uptake at high $[\text{Ca}^{2+}]$ in MICU1KO cells (17–20). This led to a conclusion that the MICU1 function is to set the threshold for Ca^{2+} uptake via mtCU at low $[\text{Ca}^{2+}]$ (20, 21), while enhancing it at high $[\text{Ca}^{2+}]$ (20). MICU1 coimmunoprecipitation with MCU (5, 19) and mutational analysis suggested that MICU1 prevents Ca^{2+} uptake via mtCU at low $[\text{Ca}^{2+}]$ by electrostatically interacting with MCU and physically blocking the pore (22, 23). This was later confirmed in two human and beetle mtCU structures with human MICU1 in the presence and absence of Ca^{2+} (24–26). A fourth structure showed only one state for mtCU with MICUs (27), which is similar to the structure obtained at high $[\text{Ca}^{2+}]$ in the other studies.

MICU1 functioning in the mtCU at high $[\text{Ca}^{2+}]$ is difficult to isolate from possible involvements of EMRE (28, 29), whereas its operation at resting low nanomolar physiological cytoplasmic $[\text{Ca}^{2+}]$ remains poorly studied due to technical limitations. The threshold (or set point) for mitochondrial Ca^{2+} uptake was well known before from studies on isolated mitochondria (30, 31) and is currently attributed to the occlusion of the mtCU pore by MICU1 when its EF-hands are unoccupied by Ca^{2+} (21). However, little is known about ion permeation via mtCU under these conditions. A well-known approach to estimate Ca^{2+} channel properties at low $[\text{Ca}^{2+}]$ is to study permeation of monovalent ions in divalent-free conditions (32, 33). In the past, this allowed clarification of the gating mechanism and ion permeation through the pore for several Ca^{2+} channels that were found to readily conduct Na^+ in the absence of divalent ions (32, 33).

Significance

Calcium enters mitochondria via calcium uniporter and regulates cellular energy production and survival. The uniporter activity is tightly regulated by calcium that changes the channel functioning mainly by binding EF-hands of the regulatory MICU subunits. However, there is a controversy on how exactly this is implemented. Particularly, little is known on MICU1 and channel functioning in low-calcium conditions. We have demonstrated that MICU1 prevents ion permeation through the uniporter in divalent-free conditions, but MICU1-free channels seem to occur even in cells with high MICU1 abundance. Our finding is important for better understanding of the uniporter functioning in cells at resting calcium concentrations and for development of channel modulators as their action is often MICU1 dependent.

Author affiliations: ^aMitoCare Center, Department of Pathology, Anatomy and Cell Biology, Thomas Jefferson University, Philadelphia, PA 19107

Author contributions: M.R.-P., E.B., and G.H. designed research; M.R.-P., E.B., M.T.C., M.P., and G.H. performed research; S.L.M.-F. contributed new reagents/analytic tools; M.R.-P., E.B., M.T.C., and M.P. analyzed data; and M.R.-P., E.B., and G.H. wrote the paper.

The authors declare no competing interest.

This article is a PNAS Direct Submission.

Copyright © 2023 the Author(s). Published by PNAS. This article is distributed under [Creative Commons Attribution-NonCommercial-NoDerivatives License 4.0 \(CC BY-NC-ND\)](https://creativecommons.org/licenses/by-nc-nd/4.0/).

¹M.R.-P. and E.B. contributed equally to this work.

²To whom correspondence may be addressed. Email: Gyorgy.hajnoczky@jefferson.edu.

This article contains supporting information online at <https://www.pnas.org/lookup/suppl/doi:10.1073/pnas.2218999120/-/DCSupplemental>.

Published May 1, 2023.

The ability of intact energized mitochondria to conduct monovalent ions in the absence of divalent ions was studied since the 1960s (34–39). An electrogenic uniport pathway for monovalent ions was suggested with selectivity similar to mtCU, $\text{Li}^+ > \text{Na}^+ > \text{K}^+$, by directly measuring Na^+ and K^+ inside mitochondria using atomic absorption microscopy, estimating mitochondrial swelling by light scattering, and measuring mitochondrial depolarization and respiration increase (34, 36, 38–40). These studies also suggested the presence of passive outflow pathway along the concentration gradient possibly via Na^+/H^+ exchange mechanism (38, 41). Na^+ flux via mtCU in divalent-free conditions was proposed in 1990 after measuring Ruthenium Red-sensitive Na^+ -induced swelling, drop in the membrane potential, and increase in respiration in energized mitochondria (41) and was recently confirmed by the lack of mitochondrial depolarization in MCU knockout (MCUKO) under these conditions (42).

A groundbreaking study explored the electrophysiological properties of the mtCU using isolated mitoplasts and demonstrated that the channel selectivity to monovalent ions in divalent-free conditions is similar to that described for isolated mitochondria ($\text{Na}^+ > \text{K}^+$) (40). Na^+ conductance has been shown to be efficiently suppressed by 10 nM or less $[\text{Ca}^{2+}]_c$ in mitoplasts from COS-7 cells and mouse embryonic fibroblasts (MEFs) with a complete block at 100 nM (40, 42). A similar value of 10 nM has been recently shown to prevent Na^+ conductance in MICU-free MCU–EMRE complex from *Tribolium castaneum* in a reconstituted lipid bilayer system (43). Further patch-clamp studies of the mtCU's Na^+ conductance in isolated mitoplasts reported complicated matrix regulation of the channel properties (44, 45). A recent work focused on the MICU1's role in mtCU gating and ion permeation in divalent-free conditions using both patch-clamp characterization of wild-type (WT) and MICU1KO mtCU's Na^+ conductance in isolated mitoplasts and measuring the Na^+ influx-induced depolarization in intact mitochondria (42). MICU1 was found to be unable to regulate the Na^+ influx via mtCU, and reconsidering the mechanism of MICU1-dependent gating of the mtCU was suggested. However, the study has some limitations related to the use of mitoplast preparation (46) and to the lack of consideration of possible mtCU rearrangements in MICU1's absence.

In the present study, we set out to test the MICU1-dependent mtCU gating and ion permeation in divalent-free conditions in intact mitochondria in suspensions of permeabilized cells and in adherent single permeabilized cells by estimating Na^+ influx using different fluorescence-based approaches and side scattering (SSC) in WT, MICU1KO, and different rescues. Our goal was also to evaluate whether possible discrepancies among previously published data might be caused by mtCU rearrangement in the absence of MICU1 and limitations of the mitoplast preparation.

Results

MICU1 Controls the Na^+ Flux-Mediated Mitochondrial Depolarization and Swelling in Permeabilized HEK Cells. Biochemical and structural evidence supports that MICU1 binds to MCU to suppress the cation flux through the mtCU pore at $[\text{Ca}^{2+}]$ too low to saturate its EF-hands (17, 22, 24). However, this model was challenged recently partly based on data showing the lack of MICU1-dependent suppression of the mtCU-mediated Na^+ flux measured by the accompanying mitochondrial depolarization upon Ca^{2+} and Mg^{2+} removal in isolated mitochondria (42). To further investigate this matter, we set up monitoring the mitochondrial depolarization, swelling, and $[\text{Na}^+]$ (free sodium concentration) increase in the mitochondrial matrix following mtCU-mediated Na^+ uptake in divalent-free conditions in HEK293T cells of

three genotypes: WT, MICU1 knockout (M1KO), and stable rescue of M1KO with MICU1-HA (M1Rs).

First, cell suspensions for each line were permeabilized in a Ca^{2+} - and K^+ -free medium containing 130 mM Na^+ . The mitochondrial membrane potential ($\Delta\Psi_m$) and matrix volume were simultaneously monitored by a fluorescent potentiometric dye, tetramethyl rhodamine (TMRM), and SSC, respectively (Fig. 1 *A–I* and *SI Appendix, Fig. S1*). The addition of succinate powered the generation of a stable $\Delta\Psi_m$ that was similar for each genotype. Then, EDTA was added to chelate Mg^{2+} and the remaining Ca^{2+} , and in turn to induce mitochondrial Na^+ influx (39). This resulted in mitochondrial depolarization in all genotypes but it was faster and larger in M1KO than that in WT and M1Rs (Fig. 1 *A–C*, *G*, and *H* and *SI Appendix, Fig. S1*).

After stabilization of $\Delta\Psi_m$ at a new level, a Na^+ ionophore gramicidin was added to maximize the Na^+ influx (Fig. 1 *A–C* and *SI Appendix, Fig. S1 A–C*). Gramicidin caused additional depolarization only in WT and M1Rs having no effect in M1KO, which indicates the MICU1 role in the limitation of the Na^+ entry into mitochondria. In the end of each experiment, an uncoupler, carbonyl cyanide p-trifluoro methoxyphenylhydrazone (FCCP), was added to ensure complete dissipation of $\Delta\Psi_m$ (*SI Appendix, Fig. S1 A–C*). Ru265, an mtCU blocker (47), suppressed the EDTA-induced mitochondrial depolarization in each genotype, confirming that it was caused by Na^+ influx across the mtCU (Fig. 1*H*). However, Ru265 suppressed EDTA-induced depolarization more efficiently in M1KO than that in WT and M1Rs (Fig. 1*H*), which can be due to less efficient inhibition of MCU by ruthenium-based compounds in the presence of MICU1 reported previously (22). Another possibility is the presence of another Na^+ entry pathway when mtCU is blocked/absent as the presence of Ruthenium Red-insensitive Na^+ influx was also shown in intact mitochondria from MCUKO and WT, but not MICU1KO MEFs by Garg et al. (42).

Na^+ uptake also induces an increase in the volume of the mitochondrial matrix that can be monitored by light or SSC (48). The SSC recorded simultaneously with $\Delta\Psi_m$ indicated a greater swelling in M1KO than that in either WT or M1Rs, and gramicidin caused additional swelling only in WT and M1Rs (Fig. 1 *D–F* and *I*), providing further evidence of MICU1-mediated suppression of the Na^+ influx. Ru265 prevented the EDTA-induced mitochondrial swelling in each genotype (Fig. 1*I*).

In the end of the $\Delta\Psi_m$ and matrix volume measurements, the cells' membrane fraction was recovered by centrifugation and used to estimate mtCU components by immunoblot (Fig. 1 *J–M*). MICU1 was absent in M1KO and was rescued beyond its WT level in M1Rs (Fig. 1 *J* and *K*). Notably, MICU1 deletion was also associated with ~80% decrease in MICU2, ~50% in MCU, and ~95% in EMRE (Fig. 1 *J* and *L–M*). M1Rs had all the mtCU components, but MCU restored close to the normal levels (Fig. 1 *J–N*).

Altogether, this suggests that the EDTA-induced mtCU-mediated Na^+ influx is unrestricted only in M1KO mitochondria even with the robust EMRE downregulation that is predicted to reduce the amount of the functional mtCU pores.

MICU1 Controls the Na^+ Influx-Induced Mitochondrial Matrix $[\text{Na}^+]$ Increase in Adherent Permeabilized HEK Cells. To measure Na^+ directly, we loaded the cells with a ratiometric Na^+ -sensing fluorescent dye, sodium-binding benzofuran isophthalate (SBFI), using the acetoxymethyl ester (49). A part of SBFI gets trapped in the mitochondria (50, 51) and allows measurement of matrix $[\text{Na}^+]$ ($[\text{Na}^+]_m$) upon permeabilization of the plasma membrane by saponin and washing out of the cytoplasmic SBFI. Cells were also loaded with TMRM to monitor $\Delta\Psi_m$ (Fig. 2 and *SI Appendix, Fig. S2*). Single-cell imaging showed the same differences in

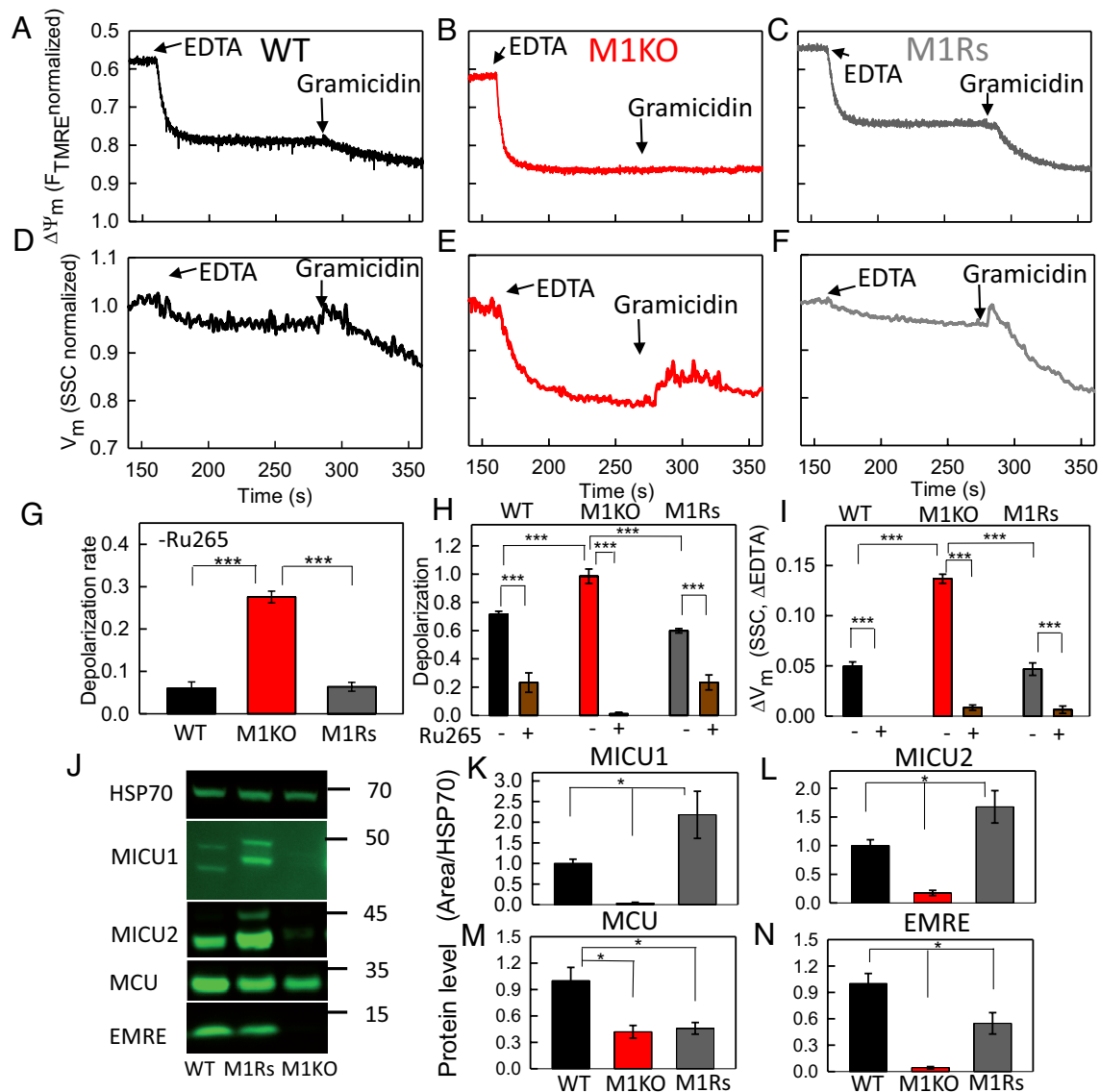


Fig. 1. MICU1 controls the Na^+ influx-induced mitochondrial depolarization (A–C) and swelling (D–F) in permeabilized HEK cells. Na^+ influx into mitochondria was induced by depleting Mg^{2+} and Ca^{2+} with EDTA (0.5 mM). Subsequently, gramicidin (1 μM) was added to maximize the Na^+ influx. In the end, an uncoupler, FCCP (2 μM), was added to attain complete dissipation of $\Delta\Psi_m$ (SI Appendix, Fig. S1). Ru265-sensitive EDTA-induced initial depolarization rate (G) was calculated as $dF_{\text{normalized}}/dt$ ($t = 0$) with Ru265-insensitive part subtracted [N (WT) = 5, N (M1KO) = 8, N (M1Rs) = 9]. EDTA-induced depolarization relative to the complete depolarization (H) was calculated as $\Delta F_{\text{EDTA}}/\Delta F_{\text{FCCP}}$ [N (WT/Ru265) = 14/5, N (M1KO/Ru265) = 13/4, N (M1Rs/Ru265) = 12/4]. EDTA-induced mitochondrial swelling (I) is estimated [N (WT/Ru265) = 24/6, N (M1KO/Ru265) = 35/19, N (M1Rs/Ru265) = 27/11]. The cells' membrane fractions from the experiments [N (WT) = 9, N (M1KO) = 8, N (M1Rs) = 6] were used for immunoblotting (J). MICU1 (K), MICU2 (L), MCU (M), and EMRE (N) levels relative to HSP70 were calculated. MW in (J) is indicated in kDa. Traces in (A–C) were normalized to $F[\text{TMRE}]_{\text{FCCP}1.1}$. Traces in (D–F) were normalized to the baseline. Data were compared using two-way (H and I) and one-way (G and K–N) ANOVA with Holm–Sidak Post Hoc test. For (K–N), the lowest significance level is indicated. MEAN \pm SEM, * $P < 0.05$, ** $P < 0.01$, *** $P < 0.001$.

Na^+ -induced mitochondrial depolarization among WT, M1KO, and M1Rs (Figs. 2 and 3 and SI Appendix, Fig. S2), which were observed by fluorometry in the corresponding cell suspensions in Fig. 1 A–C, G, and H and SI Appendix, Fig. S1. During the imaging, we used FCCP to attain complete dissipation of $\Delta\Psi_m$ following EDTA addition, and it depolarized mitochondria further in WT and M1Rs, but did not have any effect in M1KO (Fig. 2 E–G and SI Appendix, Fig. S2 A–C). Alamethicin, a channel forming ionophore that can mediate Na^+ flux (52) independent of the mtCU, when added instead of the uncoupler, also further depolarized mitochondria only in WT and M1Rs (SI Appendix, Fig. S3 A–C). Thus, these results extend the indirect evidence of the MICU1 role in the suppression of the mitochondrial Na^+ influx in divalent-free conditions.

Recording $[\text{Na}^+]_m$ showed an increase upon EDTA addition in all genotypes, but it was faster in M1KO than that in WT or M1Rs

(Fig. 2 A–D). Both EDTA-induced mitochondrial depolarization and $[\text{Na}^+]_m$ increase were prevented by Ru265 (Figs. 2 I–K and 3A and SI Appendix, Fig. S4). Thus, our results provide a broad support for Na^+ traversing the mtCU pore upon Ca^{2+} and Mg^{2+} removal, leading to mitochondrial depolarization and swelling in HEK293T cells. However, both the endogenously expressed MICU1 in WT and MICU1 reexpressed in a stable manner in M1KO suppress the Na^+ influx and its consequences in terms of $\Delta\Psi_m$ and matrix volume changes.

Great Abundance of MICU1 or Its EF-Hand Mutant Prevents the mtCU Na^+ Flux. An unexpected result of our studies was that endogenous/stably expressed MICU1 did not completely prevent Na^+ entry and the ensuing mitochondrial depolarization and swelling (Figs. 1–3). To test whether this occurred because not every mtCU was gated by MICU1, acute overexpression of

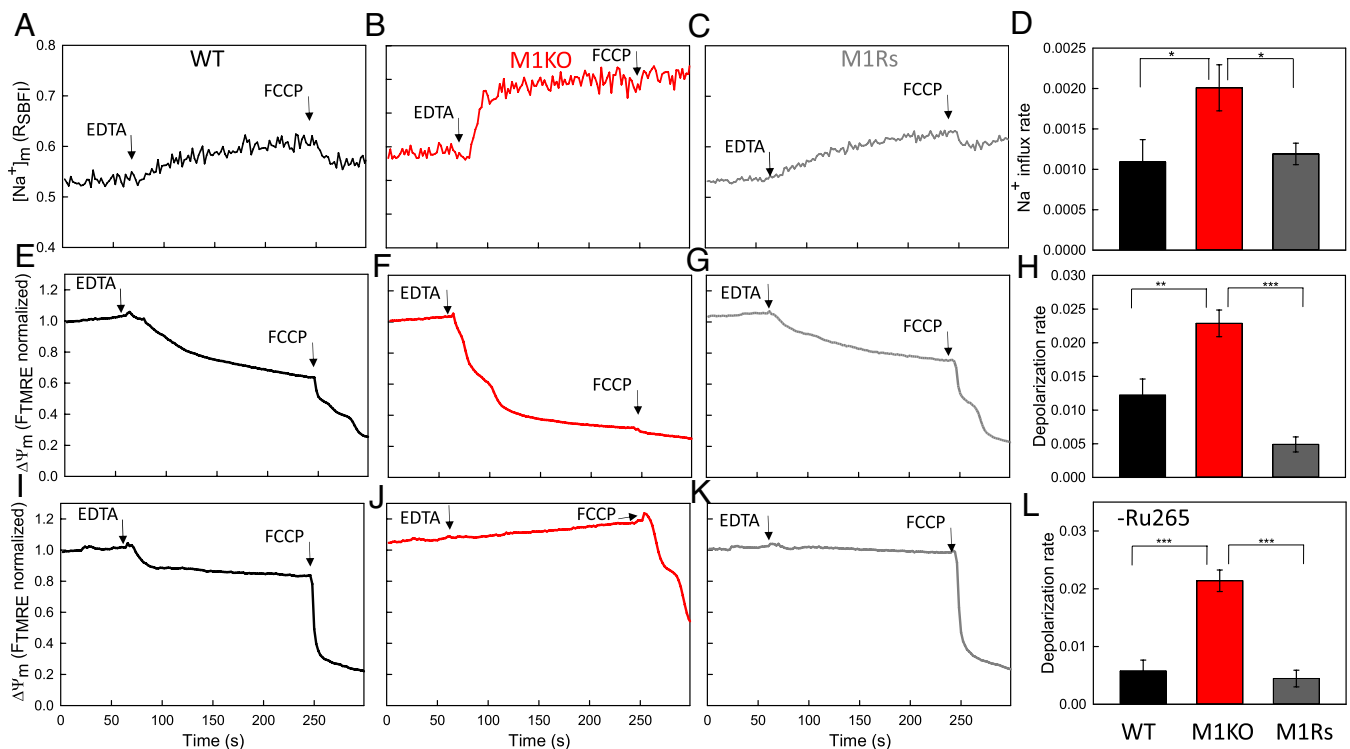


Fig. 2. MICU1 controls the Na^+ influx-induced $[Na^+]_m$ increase (A–C) and the accompanying depolarization (E–G) in adherent permeabilized HEK cells. Na^+ influx into mitochondria was induced by depleting Mg^{2+} and Ca^{2+} with EDTA (0.5 mM) in the indicated genotypes in the absence (A–C and E–G) and presence of Ru265 (3 μ M) (I–K). Initial EDTA-induced Na^+ influx rate (D) was calculated as $dRSBFI/dt$ ($t = 0$) ($N = 5$). Initial EDTA-induced mitochondrial depolarization (H and L) was calculated as $-dF_{normalized}/dt$ ($t = 0$) without (H) and with (L) subtraction of Ru265-insensitive part [$N(WT) = 7$; $N(M1KO) = 11$; $N(M1Rs) = 4$]. An uncoupler, FCCP (2 μ M), was added in the end to attain complete dissipation of $\Delta\Psi_m$. Traces in (A–C, E–G, and I–K) were normalized to the baseline. Data were compared using one-way ANOVA with Holm–Sidak Post Hoc test. For (D), comparisons against the control group (M1KO) were made. MEAN \pm SEM, * $P < 0.05$, ** $P < 0.01$, *** $P < 0.001$.

MICU1 was established in M1KO (48 h, M1Ra), which resulted in >10-fold higher MICU1 abundance over the WT and M1Rs levels (SI Appendix, Fig. S5). In M1Ra, EDTA did not induce any Ru265-sensitive mitochondrial depolarization (Fig. 3 and SI Appendix, Fig. S6). Similarly, acutely overexpressed MICU1 EF-hand mutant (M1_{EFm}Ra) that fails to bind Ca^{2+} completely inhibited the EDTA-induced Ru265-sensitive depolarization (Fig. 3 and SI Appendix, Fig. S6). Importantly, in some of these acute rescue experiments, bicistronic constructs of MICU1/MICU1_{EFm} and mRFP were used, which allowed identification of the rescued cells and direct validation of the different patterns of the EDTA-induced depolarization in rescued and nonrescued cells in the same imaging field (SI Appendix, Fig. S6). The quantification of the EDTA-induced depolarization and its sensitivity to Ru265 for each genotype (WT, M1KO, M1Rs, M1Ra, M1_{EFm}Ra) are shown side by side in Fig. 3. While mtCU abundance is greatly reduced in M1KO, acute MICU1 overexpression partially restored WT mitochondrial Ca^{2+} uptake phenotype both at high and low Ca^{2+} concentrations (22) (Fig. 4), having even more profound effect on the Na^+ influx. Thus, the mtCU Na^+ influx might be fully prevented by great levels of MICU1 or its Ca^{2+} -insensitive mutant.

EMRE Loss in M1KO Cells Limits the mtCU Cation Flux Capacity.

To directly address the role of the secondary EMRE decrease in the MICU1KO mtCU phenotype, the M1KO HEK cells were rescued acutely (48 h) with either MICU1 (M1Ra) or EMRE (ERa) (Fig. 4). MICU1 reintroduction increased MICU1, MICU2, and EMRE, whereas EMRE only increased EMRE, and neither MICU1 nor EMRE affected MCU (Fig. 4 D–H and SI Appendix, Fig. S5).

The WT, M1KO, M1Ra, and ERa cells were permeabilized in suspension, and their mitochondrial Ca^{2+} uptake was tested by

monitoring Ca^{2+} clearance during a 2-pulse protocol. First, a small Ca^{2+} bolus (low Ca^{2+} , 7 μ M $CaCl_2$) to test the mtCU gatekeeping was added and after 2 min, it was followed by a large Ca^{2+} bolus (high Ca^{2+} , 25 μ M $CaCl_2$) to estimate the maximal mitochondrial Ca^{2+} uptake capacity (Fig. 4 A–C). Consistent with our and others' findings in several cell types/tissues (19, 20, 53–56), MICU1 reexpression tended to decrease the Ca^{2+} uptake at low Ca^{2+} and greatly increased it at high Ca^{2+} (Fig. 4 A–C), partially restoring WT phenotype as has been shown before (22). Differently, EMRE expression increased the Ca^{2+} uptake at both low and high Ca^{2+} (Fig. 4 A–C). This was further supported by a finding that MICU1 rescue suppressed Na^+ -induced mitochondrial depolarization in divalent-free conditions, while EMRE rescue increased its rate when measured as described previously (SI Appendix, Fig. S7A). Since neither MICU1 nor EMRE rescue affected MCU and both MICU1 and EMRE increased the Ca^{2+} uptake capacity, these results suggest that EMRE loss caused a decrease in the amount of the functional mtCU channels. Altogether, this indicates that a secondary EMRE reduction in MICU1 deficient cells can contribute to the decrease in their maximal mitochondrial Ca^{2+} uptake capacity, whereas MICU1 affects the mtCU gating by occluding the pore at low $[Ca^{2+}]$ and possibly enhancing the flux at high $[Ca^{2+}]$.

Notably, MICU1 loss is associated with EMRE decrease in many different paradigms, including MICU1KO patient lymphoblasts, murine liver, skeletal muscle, and brain (55–58). MICU1KO embryonic fibroblasts also display greatly reduced EMRE abundance and have mitochondrial Ca^{2+} uptake phenotype similar to M1KO HEK293 (SI Appendix, Fig. S7 B–E). MICU1 role in the mtCU occlusion when its EF hands are unoccupied in both cell lines is confirmed by a complete block of Ca^{2+} entry to mitochondria upon expression of MICU1 EF-hand

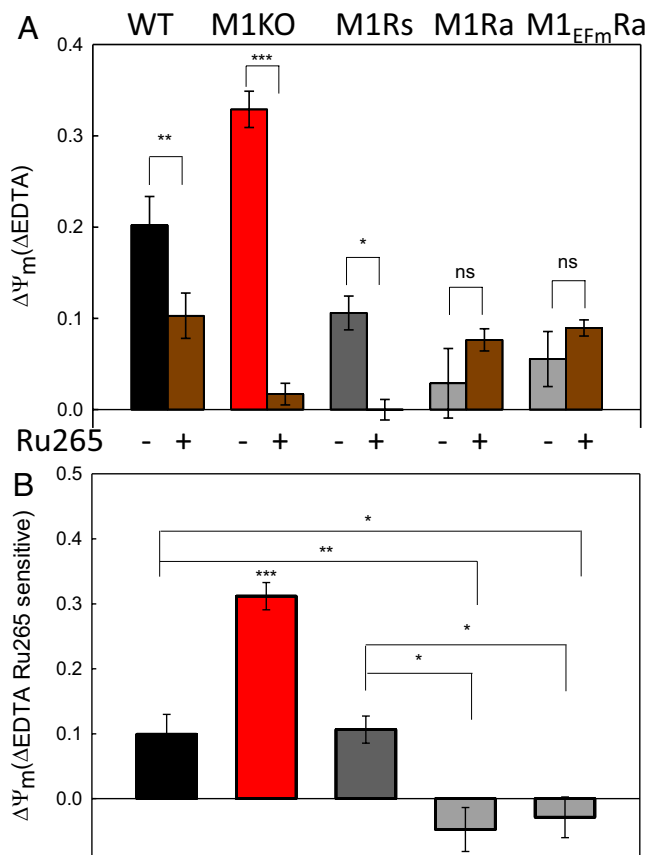


Fig. 3. Great abundance of MICU1 or its EF-hand mutant prevents the mtCU Na^+ influx. Mitochondrial depolarization induced by Na^+ entry following EDTA (0.5 mM) addition in divalent-free conditions in the indicated genotypes in the presence and absence of Ru265 (3 μM) calculated as difference in $\Delta\Psi_m$ between 90 s and 54 s for Fig. 2 and similar experiments with acute rescues [N(WT) = 7; N(M1KO) = 11; N(M1Rs) = 4; N = 4(M1Ra); N(M1_{EFm}Ra) = 4] (A). Ru265-sensitive EDTA-induced mitochondrial depolarization calculated from A (B). Data were compared using two-way ANOVA with Holm-Sidak Post Hoc test. MEAN \pm SEM, * P < 0.05, ** P < 0.01, *** P < 0.001.

mutants [(17) and *SI Appendix, Fig. S7D*]. Thus, EMRE decrease can broadly contribute to the mtCU channel abundance in MICU1-deficient cells.

The mtCU Complex Can Lose MICU1 during Isolation of Mitoplasts. Patch-clamp is a powerful electrophysiological technique that makes it possible to examine channel properties by strictly controlling the environment and membrane potential/current. Ion channels in the inner mitochondrial membrane (IMM) are inaccessible for the patch-clamp pipette in intact mitochondria, and their study requires the use of mitochondria with ruptured outer membrane, mitoplasts (40). However, mitoplasts have IMM exposed to extramitochondrial medium, and it is hard to exclude alterations in the functioning of proteins that normally operate in the mitochondrial intermembrane space (IMS). mtCU is an IMM channel that is gated by its IMS components, MICUs (20, 59). To estimate how OMM (outer mitochondrial membrane) loss affects MICU1, M1Rs HEK transfected with a mitochondrial matrix marker, mtDsRed, were fractionated to permeabilized cells, mitochondria, and mitoplasts using French press (Fig. 5A). Further, MICU1-HA abundance in different preparations was evaluated by colocalization with mtDsRed using immunofluorescent staining (Fig. 5B and C). The specificity was controlled by omitting the secondary antibody staining step (*SI Appendix, Fig. S8*), and the specificity of the primary anti-HA antibody was tested by immunoblotting M1KO,

WT, M1Rs, and M1Ra HEK cells (*SI Appendix, Fig. S9*). Though French press allowed gentle preparation of mitoplasts without a significant loss in cytochrome *c* (*SI Appendix, Fig. S10*), it led to MICU1 loss in the mitoplast estimated by MICU1 colocalization with mitochondrial matrix (Fig. 5C).

To test whether MICU1 loss leads to an increase in MICU1-free mtCU, mitochondria and mitoplasts isolated from WT and M1KO HEK were analyzed by Blue native-polyacrylamide gel electrophoresis (BN-PAGE, Fig. 6A and B). Mild detergent conditions (1% 1 g/g digitonin) were used for solubilization as they have been previously reported to yield predominantly MICU1-containing mtCU complexes in WT HEK mitochondria with MW around 1 MDa (60), which is in good agreement with approximate MW of mtCU dimers with MICUs reported in structures (24–27). WT mitoplasts showed less MICU1 in ~1 MDa mtCU complexes (Fig. 6A) and a shift of mtCUs probed by MCU to lower MW regions including regions corresponding to MICU1-free mtCUs (Fig. 6B) when compared to the corresponding mitochondria. mtCUs in M1KO mitoplasts and mitochondria were not significantly different from each other (Fig. 6B). They showed very low-abundant complexes around 720 kDa that correspond well to MW of EMRE-containing mtCU dimers (61) and high-abundant complexes below 480 kDa that are in good agreement with MW of EMRE-free mtCU complexes previously reported to coincide by size with those in EMREKO HEK (6) and unable to form mtCU dimers (61) (Fig. 6B). Solubilized mitochondrial and mitoplast proteins from Fig. 6A and B were further analyzed by SDS-PAGE in reducing conditions and immunoblotted against MICU1 and MCU (Fig. 6C and D). WT mitoplasts showed reduced MICU1 abundance at unaltered MCU level (Fig. 6C and D). Since French press preparation contains mitochondria with intact and ruptured OMM (62), we conclude that these MICU1-free MCUs are likely to be present in mitoplasts with ruptured OMM. Altogether, this indicates that the results of patch-clamp characterization of MICU1-dependent gating of mtCU in mitoplasts should be taken cautiously, and loss of MICU1 should be carefully considered.

Discussion

We have demonstrated that MICU1 prevents ion permeation through the mtCU pore when its EF-hands are unoccupied by Ca^{2+} and only MICU1-free mtCUs are capable of mediating Na^+ flux in the absence of Ca^{2+} . We further showed that MICU1-free mtCUs might be present even in HEK293 cells where mtCUs are heavily gated by MICU1 and the threshold for mitochondrial Ca^{2+} uptake is close to the micromolar range (17, 22, 63). Thus, our finding is important for understanding ion permeation through mtCU and its MICU1-dependent gating in different cell types.

MICU1 function to exert Ca^{2+} -dependent regulation of Ca^{2+} uptake via mtCU is widely accepted. While most fluorimetry and radioactive assays of mitochondrial Ca^{2+} uptake together with structural studies suggest that MICU1 gates mtCU by physically occluding the pore at low Ca^{2+} , a recent study by Garg et al. challenged this model by reporting on unaltered Na^+ flux in the absence and presence of MICU1 both in MEF-intact mitochondria and mitoplasts by measuring mitochondrial depolarization and Na^+ conductance in divalent-free conditions (42). The ability of mtCU in WT mitochondria to mediate monovalent flux in the absence of Ca^{2+} and Mg^{2+} and thus with unoccupied MICU EF-hands was recognized long before molecular identification of mtCU by indirect measurements of Ruthenium Red-sensitive mitochondrial depolarization, swelling, and respiration increase

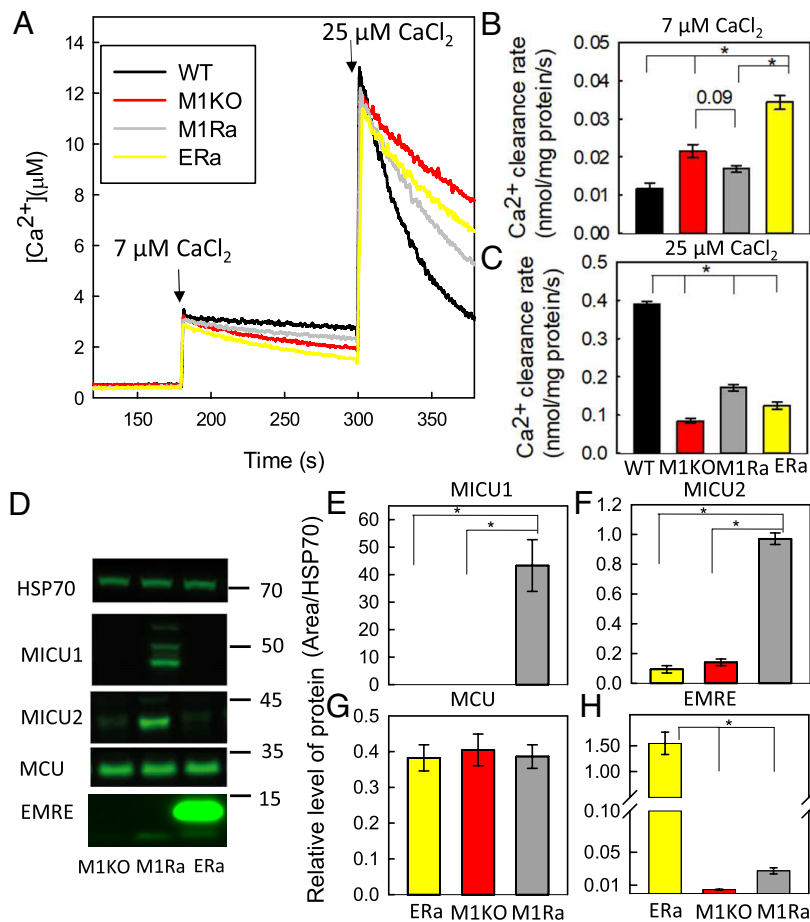


Fig. 4. EMRE loss in M1KO cells limits the mtCU cation flux capacity. Ca²⁺ clearance was tested in WT, M1KO, M1Ra, and ERa permeabilized cells following consecutive additions of 7 μM CaCl₂ and 25 μM CaCl₂ to test the mtCU gatekeeping and to estimate the maximal mitochondrial Ca²⁺ uptake capacity, respectively (A). The corresponding Ca²⁺ clearance rates (B and C) were calculated [N(WT) = 3, N(M1KO) = 15; N(M1Ra) = 10; N(ERa) = 10]. The cells' membrane fractions from the experiments were used for immunoblotting (N = 3) (D). MICU1 (E), MICU2 (F), MCU (G), and EMRE (H) levels relative to HSP70 were calculated. MW in (D) is indicated in kDa. Data were compared using one-way ANOVA with Holm-Sidak Post Hoc test, and the lowest significance level is indicated, MEAN ± SEM, *P < 0.05.

(41). We directly correlated Ru265-sensitive mitochondrial Na⁺ accumulation to accompanying depolarization and swelling in intact mitochondria. We showed that MICU1 abolishes the Na⁺-flux via mtCU and the proportion of the MICU1-free and MICU1-associated mtCU pores determines mitochondrial Na⁺ uptake by measuring single-cell mitochondrial depolarization in WT, MICU1KO, and stably and acutely MICU1 rescued cells. Thus, all our findings come together in support of Ca²⁺-free MICU1 keeping the mtCU pore closed.

Why was the occlusion of the mtCU pore by MICU1 undetectable in the mitoplast electrophysiology studies of Garg et al. (42)? MICU1 has no transmembrane domain, and we reasoned that it might get disengaged from the mtCU pore when the OMM breaks and through its hole the IMM squeezes through and becomes available for patching. We prepared mitoplasts using French press following the protocol of Garg et al. (42) and evaluated MICU1 by immunocytochemistry down to the single mitoplast level. The largely preserved cytochrome c staining confirmed that the inner membrane insult was mild. Still, we documented loss of MICU1. BN-PAGE analysis further demonstrated that French press-derived mitoplasts have a larger fraction of MICU1-free mtCUs than mitochondria. Thus, even if patch-clamp allows selection of the healthiest objects, it is difficult to exclude alterations in MICU1 abundance and functioning after the IMM herniates across the outer membrane and gets exposed to osmotic differences and numerous changes

in solutions. This might be a factor contributing to the lack of MICU1 gatekeeping in the report of Garg et al and to the varying results reported by separate groups on mitoplasts isolated from MICU1KO and WT MEF, HeLa, and HEK293 even at high [Ca²⁺] with Ca²⁺ as the charge carrier (42, 45, 64, 65). Patch-clamp is the gold standard for studying ion channels, but the above-mentioned complications in the study of IMM channels including nonintegral IMS components deserve a consideration.

Why was a decrease documented in the Ca²⁺ conductance in the MICU1-KO by Garg et al. (42)? This phenotype might reflect the loss of a positive regulation by the Ca²⁺-bound MICU1, but a possible confounding factor is the mtCU complex rearrangement that occurs upon deletion and reintroduction of MICU1. Specifically, we showed that MICU1 deletion in HEK293 reduces the amount of functional mtCU channels probably because of a dramatic decrease in EMRE abundance. And even acute MICU1 rescue elevates EMRE. Furthermore, EMRE rescue alone enhances the mtCU Na⁺ flux in the M1KO. In terms of the mtCU Ca²⁺ flux, EMRE rescue increased mitochondrial Ca²⁺ uptake proportionally at low and high [Ca²⁺], whereas MICU1 only increased the Ca²⁺ uptake at high [Ca²⁺] like shown in ref. 66. It should be also noted that while EMRE downregulation is observed in many MICU1-deficient models including human fibroblasts, Bhosale and coauthors observed its upregulation in patients with loss-of-function MICU1 mutation (67). Thus, regarding the effect

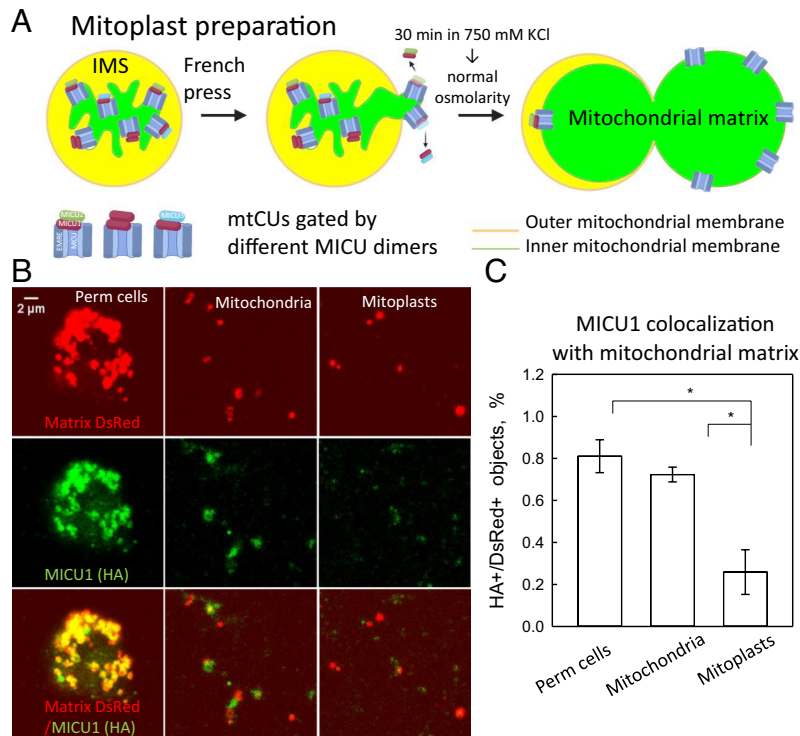


Fig. 5. Mitoplasts during isolation can lose MICU1. M1Rs cells transfected with mitochondrial matrix marker, mtDsRed, were fractionated to permeabilized (perm) cells, mitochondria, and mitoplasts as indicated (A) and immunostained against HA-tagged MICU1. The corresponding images for mtDsRed and HA-tagged MICU1 signals and merged signals are shown (B). Colocalization of mtDsRed and HA-tagged MICU1 was estimated by percentage of objects that had both mtDsRed and HA signals (HA+/DsRed+) (N = 3) (C). Experiment was performed three times; minimum three fields with more than 20 objects per condition in one experiment were analyzed. Data were compared using one-way ANOVA with Holm-Sidak Post Hoc test; the lowest significance level is indicated, MEAN ± SEM, **P* < 0.05.

of MICU1-KO and MICU1 rescue on the mtCU Ca^{2+} conductance, changes in EMRE and possibly in other mtCU components the abundance of which is altered by MICU1 seem to require some attention.

Our finding that in WT HEK some mtCU escape gatekeeping by MICU1 was unexpected because HEK cells are among the cells with high MICU1 abundance. This group of cells also includes the MEFs and hepatocytes, but other cells like those in the striated muscle have low MICU1 relative to MCU (54, 66) and likely more MICU1-free mtCU. MICU1's presence in mtCU has been reported to be ensured during assembly by mAAA proteases that can degrade MICU-free, but not MICU-bound, EMRE subunits

(60, 63). Therefore, it is possible that a very small fraction of MICU-free EMRE subunits can avoid degradation and form MICU-free mtCUs that can be seen in BN-PAGE analysis of WT HEK by us and others (60). Furthermore, a large suppression of Na^+ influx by MICU1 despite drastic downregulation of mtCUs in MICU1KO indicates that the amount of MICU1-free mtCU in WT HEK is indeed very small. Thus, the variability in MICU1-free mtCUs among different cell types is one factor that can underlie variation in MICU1KO phenotypes. Future research is required to identify the benefits of keeping a fraction of the mtCU MICU1-free and creating heterogeneity in the mtCU gating within and among cells.

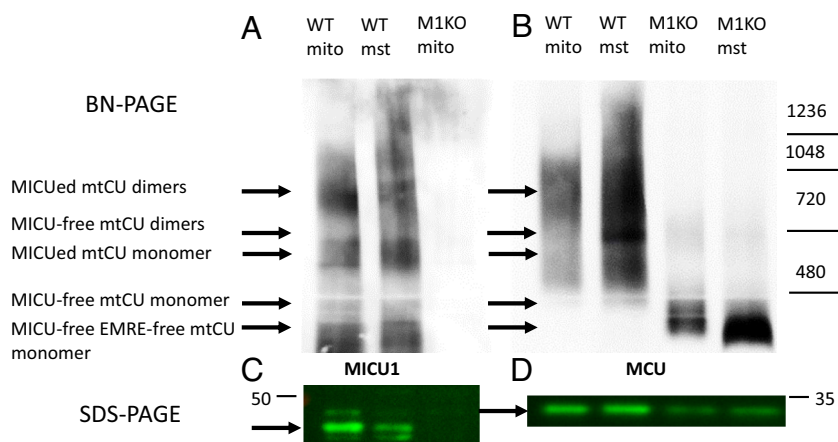


Fig. 6. The mtCU complex can lose MICU1 during isolation of mitoplasts. WT and M1KO cells were fractionated to mitochondria and mitoplasts as indicated in Fig. 5A. The mitochondria (100 μg) and mitoplasts (50 μg) were solubilized with 1% digitonin (1 g/g) and analyzed by BN-PAGE followed by immunoblotting against MICU1 (A) and MCU (B). The abundance of MICU1 (C) and MCU (D) for (A) and (B) was analyzed by SDS-PAGE in reducing conditions (20 μg mitochondria and 10 μg mitoplasts were used). MW is indicated in kDa.

Methods

Cell Lines. MICU1-KO (M1KO) and the corresponding WT HEK293T were kindly provided by Vamsi Mootha and grown as previously described (6). M1KO cells were transfected with pcDNA-dest40-MICU1-HA (21) using Lipofectamine 3000 (Invitrogen) and selected with 150 $\mu\text{g}/\text{mL}$ zeocin. A single clone was isolated by limiting dilution, and M1KO cells stably expressing MICU1-HA (M1Rs) were further cultured in the presence of 150 $\mu\text{g}/\text{mL}$ zeocin.

Acute transfection of the control plasmid pcDNA3-dest40, pcDNA-dest40-MICU1-HA (21), pcDNA-dest40-M1-EF1-D9E-HA (22), EMRE-Myc (22), was performed in HEKs using Lipofectamine 3000 according to manufacturer's protocol.

Permeabilized Cell Imaging of $\Delta\Psi_m$ and $[\text{Na}^+]_m$. The cells were preincubated in a serum-free extracellular medium (ECM, 120 mM NaCl, 5 mM NaHCO_3 , 10 mM Na-HEPES, 4.7 mM KCl, 1.2 mM KH_2PO_4 , 1.2 mM MgSO_4 , 2 mM CaCl_2 , 10 mM glucose, pH 7.4) containing 2% BSA for 15 min. The cells were subsequently loaded with 10 μM SBFI AM in the presence of 0.003% pluronic acid in the same medium for 1 h at 37 $^\circ\text{C}$. Then, the cells were washed with Ca^{2+} -free ECM containing 0.25% BSA, rinsed with ECM containing 100 μM EGTA, and permeabilized with saponin (25 $\mu\text{g}/\text{mL}$) for 5 min at 37 $^\circ\text{C}$ in a Na^+ -based medium (130 mM NaCl, 1 mM NaH_2PO_4 , 20 mM HEPES/Tris, 5% dextrose, pH 7.2) supplemented with protease inhibitors (PI, pepstatin, leupeptin, antipain at 1 $\mu\text{g}/\text{mL}$), 25 nM TMRE, 2 μM thapsigargin (Tg), 30 μM EGTA, and 100 μM MgATP. After the permeabilization, the cells were washed with Na^+ -based medium to remove saponin and to include 10 nM TMRE, 2 μM Tg, 30 μM EGTA, 50 μM MgATP, and 2 mM succinate. Fluorescence wide-field imaging of $\Delta\Psi_m$ simultaneously with $[\text{Na}^+]_m$ was carried out with a ProEM1024 EMCCD (Princeton Instruments), fitted to a Leica DMI 6000B inverted epifluorescence microscope. SBFI was recorded with 340/30 nm and 380/20 nm excitation, using a 500-nm beam splitter and 540/50 nm emission, whereas TMRE with 545/20 nm excitation, 595 nm beam-splitter, and 630/60 nm emission, and an image triplet was obtained every 2 s. Na^+ influx into mitochondria was induced by depleting Mg^{2+} and Ca^{2+} with EDTA (0.5 mM) in the presence and absence of Ru265 (3 μM). An uncoupler, FCCP (2 μM), was added in the end to attain complete dissipation of $\Delta\Psi_m$. TMRE was measured in a nonquenching mode, but despite using it at nM concentrations, there were a few cells with mitochondria exhibiting dequenching upon FCCP addition; such cells were excluded from the analysis. During image analysis, the mean gray intensity for each cell was evaluated. SBFI ratio was calculated and TMRE intensity was normalized to the baseline. For estimation of initial Na^+ influx or mitochondrial depolarization rate following EDTA addition, the first 124 s or 119 s after the addition was fit to $f = y_0 + a*(1 - \exp(-b*t))$ or to $f = y_0 + a*\exp(-b*t)$ (for which we found $R^2 > 0.6$ or 0.9) and rates were estimated as $dR_{\text{SBFI}}/dt (t=0) = a*b$ or $-dR_{\text{TMRE}}/dt (t=0) = a*b$. In cases when Ru265-insensitive EDTA-induced mitochondrial depolarization was observed, its rate was calculated similarly and subtracted from total rate for the same day to get Ru265-sensitive estimate. Because SBFI loading was not always effective, some conditions were tested only by measurements of the $\Delta\Psi_m$.

Fluorimetry of $\Delta\Psi_m$, Swelling, and Mitochondrial Ca^{2+} Uptake. In the case of Ca^{2+} uptake measurements, the experiments were performed in ICM (120 mM KCl, 10 mM NaCl, 1 mM KH_2PO_4 , 20 mM Tris-HEPES at pH 7.2), whereas Na^+ -based medium was used to estimate Na^+ influx. For cell permeabilization, the media were further supplemented with 2 mM MgATP for Ca^{2+} experiments and 2 mM NaATP and 30 μM EGTA for Na^+ studies. Cell suspensions (2 mg) were permeabilized by saponin (40 $\mu\text{g}/\text{mL}$) at 37 $^\circ\text{C}$ with stirring in the presence of PI and 2 μM Tg. After the permeabilization, the cells were spun and resuspended in 1.5 mL ICM or Na^+ -based medium and maintained in a stirred thermostated cuvette at 37 $^\circ\text{C}$ in the presence of PI, 2 μM Tg, and 1 mM succinate. Ca^{2+} studies were performed in the presence of 20 μM CGP-37157 and 2 mM MgATP, whereas Na^+ experiments were performed in the presence of 5 μM EGTA and 50 μM MgCl_2 . A multiwavelength excitation dual-wavelength emission fluorimeter (DeltaRAM, PTI) was used. The extramitochondrial $[\text{Ca}^{2+}]$ was assessed using the ratiometric Ca^{2+} probe Fura-2 (formerly Fura-FF) (1 μM , TFLabs). $\Delta\Psi_m$ was measured with 1.5 μM TMRM (Invitrogen). Fura and TMRM fluorescence were recorded simultaneously using 340 to 380 nm excitation and 500 nm emission and 545 nm excitation and 580 nm emission, respectively. In Na^+ studies, TMRE fluorescence was recorded simultaneously with SSC at 520 nm. Complete depolarization (maximum dequench of TMRM fluorescence) and swelling in the case of Na^+ experiments were elicited using the

protonophore FCCP (2 μM). $\Delta\Psi_m$ traces were normalized to the fluorescence of $\text{TMRE}_{\text{FCCP}} * 1.16$. For estimation of initial mitochondrial depolarization rate following EDTA addition, 20 s after the addition were fit to $f = y_0 + a*(1 - \exp(-b*t))$ (for which we found $R^2 > 0.9$) and initial mitochondrial depolarization rate ($df/dt (t=0) = a*b$) was calculated and normalized to ΔF (FCCP—baseline prior to EDTA addition). In cases when Ru265-insensitive EDTA-induced mitochondrial depolarization was observed, its rate was calculated similarly and subtracted from total rate for the same day to get Ru265-sensitive estimate. Calibration of the Fura signal was carried out at the end of each measurement, adding 1 mM CaCl_2 , followed by 10 mM EGTA/Tris, pH 8.5. Other additions during the experiments were made without pausing the recording using Hamilton syringes. In the end of each experiment, the cells' membrane fraction was recovered by centrifugation and used to estimate mtCU components by immunoblot.

Immunoblotting. Protein lysates from cells or mitochondria were prepared in RIPA buffer supplemented with PIs and PMSF. Equivalent amounts of total protein (15 to 50 μg) were separated electrophoretically by SDS-PAGE (10% and 4-12% gels, Invitrogen) in reducing conditions and transferred to a nitrocellulose membrane (Bio-Rad). The latter was blocked in Odyssey blocking solution (Licor) for 1 h at RT and probed overnight at 4 $^\circ\text{C}$ using the following primary antibodies: anti-MICU1 (Sigma, HPA037480, 1:500), anti-MICU2 (Abcam, ab101465, 1:1,000), anti-MCU (Sigma, HPA016480, 1:500), anti-EMRE (Bethyl, A300-BL19208, 1:1,000), and anti-Hsp70 (Thermo Scientific, MA3-028, 1:1,000). After incubation with fluorescent secondary antibodies, the membranes were scanned using an Odyssey scanner (Licor). Quantification was performed using ImageJ (NIH). For BN-PAGE immunoblotting, anti-MCU (Cell signaling, 14997, 1:500), anti-rabbit HRP secondary antibody (Cell signaling, 70745, 1:2,000), and Thermo Scientific SuperSignal West Dura Extended Duration Substrate (Invitrogen) were used.

Cell Fractionation and Immunofluorescence Staining. M1Rs HEK were grown in T150 flasks in the presence of zeocin (150 $\mu\text{g}/\text{mL}$). At ~70 to 80% cell density, the medium was changed with zeocin being omitted and the cells were transfected with mtDsRed (17 μg) using Lipofectamine 3000 (Invitrogen) according to the manufacturer's instructions. Next day, the cells were split (1/10) and grown further until they reached 100% confluency in the presence of zeocin. At this point, the cells were detached by vigorous pipetting with DBPS (10 mL per flask) and centrifuged at 200 g for 5 min. The pellets were used to obtain permeabilized cells, mitochondria, and mitoplasts.

For permeabilized cell preparation, the cells were first resuspended in 10 mL Ca^{2+} -free ECM, counted, and pelleted again at 200 g for 5 min. The cells were resuspended at a concentration of 12 million/mL in ICM supplemented with PI, 2 mM MgATP, 2 μM Tg, 20 μM CGP-37157, and 10 μM EGTA and perm in the presence of ascorbate (2 mM) and TMPD (0.5 mM) by adding saponin at 40 $\mu\text{g}/\text{mL}$ for 5 min at 37 $^\circ\text{C}$ with stirring.

Mitochondria and mitoplasts were obtained according to (42). Briefly, after detachment with DPBS, cells were washed and homogenized on ice in 250 mM sucrose, 10 mM HEPES, 1 mM EGTA, and 0.1% BSA (pH adjusted to 7.2 with Trizma base) using a glass grinder with six slow strokes of a Teflon pestle rotating at 300 rpm. The homogenate was centrifuged at 700 \times g for 10 min to get rid of nuclei and cell debris. Supernatant was further centrifuged at 8,500 \times g for 10 min to get mitochondria. The mitochondrial pellet for immunofluorescent analysis was resuspended in ~200 μL ICM supplemented with PI, 2 mM MgATP, 2 μM Tg, and 20 μM CGP-37157.

For mitoplast preparation, the mitochondrial pellet was suspended in a hypertonic buffer (140 mM sucrose, 440 mM D-mannitol, 5 mM HEPES, 0.35 mM EGTA, pH adjusted to 7.2 with Trizma base) for 15 min and then subjected to a French press at 2,000 psi to rupture the OMM. The mitoplasts were centrifuged at 10,500 \times g for 10 min. The pellet (5 to 10 μL) was resuspended in 100 to 200 μL hypertonic solution (750 mM KCl, 100 mM HEPES, pH adjusted to 7.2 with Trizma base), so that the resulting EGTA content was ~17 μM and stored for 30 min. After that, the preparation was diluted with hypoosmotic buffer (5 mM sucrose, 5 mM HEPES, 1 mM EGTA, pH 7.2-tris) three times and immediately processed further.

The preparations (10 to 20 μL) were put for 5 to 10 min at 37 $^\circ\text{C}$ to 4-well-chamber slides preliminary covered with Cell-Tak (Corning) according to the manufacturer's instructions. Further, prewarmed 4% PFA was added to the slides for 15 min at RT. After 3 \times washing with PBS, the preparations were blocked in PBS solution containing 3% BSA and 0.2% triton X-100 for 30 min at RT. This was followed by 1 h incubation with anti-HA rabbit antibodies (Abcam ab9110, 1:300) at RT. After 3 \times washing with PBS containing 0.05% triton X-100, the preparations were incubated

with Goat anti-Rabbit Alexa Fluor™ Plus 647 (Thermo Fisher Scientific A32733, 1:200) for 1 h at RT. After 3 × washing with PBS containing 0.05% triton X-100, the last two steps were repeated for primary anti-cytochrome c mouse antibody (BD Biosciences 556432; 1:200) and Goat anti-Mouse Alexa Fluor™ 405 (Thermo Fisher Scientific A31553; 1:100). Negative controls were made by replacing primary antibodies with antibody dilution buffer (PBS containing 1% BSA and 0.06% triton X-100). After the final washing, the preparations were mounted in PBS and imaged using a Zeiss LSM 880 confocal microscope with 0.07 μm resolution using a 63 × objective. Excitation/emission wavelengths were: 405/450 nm for cytochrome c; 561/579 nm for mtDsRed; and 633/654 nm for MICU1-HA.

The images were analyzed in Image J. First, the background was subtracted, then for the mtDsRed channel, Otsu threshold was adjusted visually so that only meaningful objects are selected and kept constant for all images in one experiment. Prior to the thresholding, cell images were processed using “watershed (binary)” and “erode (binary).” Following thresholding, the function “analyze particles” was used to create an ROI list. This ROI list was used to measure area and intensity in MICU1-HA (HA) and cytochrome c (cytC) channels with limit to threshold adjusted and kept constant in one experiment for each channel so that only meaningful objects are selected. MtDsRed-positive (DsRed+) objects that have a nonzero area in M1-HA (HA+) and cytC(cytoC+) channels were counted and expressed in percentage from the total number of DsRed+ objects. HA+/cytoC+, HA+/cytoC-, and HA-/cytoC- objects were estimated as well.

BN-PAGE Analysis. Mitochondria (100 μg) and mitoplasts (50 μg) were solubilized in Native-PAGE sample buffer (Invitrogen) with 1% digitonin (1 g/g) for 30 min at 4 °C with shaking (1,500 rpm). Then, the solubilized proteins were cleared from the membrane fraction by spinning at 25,000 g for 20 min at

4 °C and G-250 was added to the samples at the final concentration of 0.125%. The samples were loaded to Native PAGE 3-12% Bis-Tris gels (Invitrogen) and were separated by BN-PAGE at 4 °C (Invitrogen system). Following electrophoresis, the proteins were transferred to PVDF membrane (wet transfer, 2 h at 25 V, Invitrogen system). After the transfer, the membranes were washed in 10% acetic acid/25% methanol solution for 20 min, air-dried, reactivated with methanol, and rinsed with milliQ water prior to blocking and immunostaining that was performed as described in the Immunoblotting section. Mitochondria (20 μg) and mitoplasts (10 μg) solubilized in the same way were also subjected to SDS-PAGE analysis in reducing conditions using Invitrogen system as described above.

Statistical Analysis. Data were expressed as mean ± SEM. Experiments were performed at least 2 times in duplicates or more. Statistical analysis was performed using one-way or two-way ANOVA followed by a Holm-Sidak post-hoc test. The exact number of replicates used for statistical analysis and significance is listed for each experiment in the figure legends. For immunoblot calculations and Figs. 4 and 5, the lowest significance is indicated.

Data, Materials, and Software Availability. All study data are included in the article and/or *SI Appendix*.

ACKNOWLEDGMENT. This study was funded by RO1-HL142271 to G.H. and by the Leducq Foundation MitoCardia network (16CVD04). M.P. was a recipient of a postdoctoral fellowship from the Fondation pour la Recherche Médicale (No. ARF20160936149) and American Heart Association and a grant “Aide à la mobilité” from the Institut Servier (France).

1. C. Mammucari *et al.*, Mitochondrial calcium uptake in organ physiology: From molecular mechanism to animal models. *PLoS Arch.* **470**, 1165–1179 (2018).
2. V. Granatiero, D. De Stefani, R. Rizzuto, Mitochondrial calcium handling in physiology and disease. *Adv. Exp. Med. Biol.* **982**, 25–47 (2017).
3. B. Wacquier, L. Combettes, G. Dupont, Cytoplasmic and mitochondrial calcium signaling: A two-way relationship. *Cold Spring Harb. Perspect. Biol.* **11**, a035139 (2019).
4. D. De Stefani *et al.*, A forty-kilodalton protein of the inner membrane is the mitochondrial calcium uniporter. *Nature* **476**, 336–340 (2011).
5. J. M. Baughman *et al.*, Integrative genomics identifies MCU as an essential component of the mitochondrial calcium uniporter. *Nature* **476**, 341–345 (2011).
6. Y. Sancak *et al.*, EMRE is an essential component of the mitochondrial calcium uniporter complex. *Science* **342**, 1379–1382 (2013).
7. F. Perocchi *et al.*, MICU1 encodes a mitochondrial EF hand protein required for Ca(2+) uptake. *Nature* **467**, 291–296 (2010).
8. M. Plovanich *et al.*, MICU2, a paralog of MICU1, resides within the mitochondrial uniporter complex to regulate calcium handling. *PLoS One* **8**, e55785 (2013).
9. M. Patron *et al.*, MICU3 is a tissue-specific enhancer of mitochondrial calcium uptake. *Cell Death Differ.* **26**, 179–195 (2019).
10. K. J. Kamer *et al.*, Crystal structure of MICU2 and comparison with MICU1 reveal insights into the uniporter gating mechanism. *Proc. Natl. Acad. Sci. U.S.A.* **116**, 3546–3555 (2019).
11. Y. Xing *et al.*, Dimerization of MICU proteins controls Ca(2+) influx through the mitochondrial Ca(2+) uniporter. *Cell Rep.* **26**, 1203–1212.e4 (2019).
12. K. J. Kamer, V. K. Mootha, The molecular era of the mitochondrial calcium uniporter. *Nat. Rev. Mol. Cell Biol.* **16**, 545–553 (2015).
13. J. K. Foskett, B. Philipson, The mitochondrial Ca(2+) uniporter complex. *J. Mol. Cell Cardiol.* **78**, 3–8 (2015).
14. B. R. Alevriadou *et al.*, Molecular nature and physiological role of the mitochondrial calcium uniporter channel. *Am. J. Physiol. Cell Physiol.* **320**, C465–C482 (2021).
15. W. Wu, J. Zheng, Z. Jia, Structural characterization of the mitochondrial Ca(2+) uniporter provides insights into Ca(2+) uptake and regulation. *iScience* **24**, 102895 (2021).
16. S. Feno *et al.*, The molecular complexity of the mitochondrial calcium uniporter. *Cell Calcium* **93**, 102322 (2021).
17. K. J. Kamer, V. K. Mootha, MICU1 and MICU2 play nonredundant roles in the regulation of the mitochondrial calcium uniporter. *EMBO Rep.* **15**, 299–307 (2014).
18. K. Mallilankaraman *et al.*, MICU1 is an essential gatekeeper for MCU-mediated mitochondrial Ca(2+) uptake that regulates cell survival. *Cell* **151**, 630–644 (2012).
19. M. Patron *et al.*, MICU1 and MICU2 finely tune the mitochondrial Ca2+ uniporter by exerting opposite effects on MCU activity. *Mol. Cell* **53**, 726–737 (2014).
20. G. Sordas *et al.*, MICU1 controls both the threshold and cooperative activation of the mitochondrial Ca(2+) uniporter. *Cell Metab.* **17**, 976–987 (2013).
21. K. J. Kamer, Z. Grabarek, V. K. Mootha, High-affinity cooperative Ca(2+) binding by MICU1-MICU2 serves as an on-off switch for the uniporter. *EMBO Rep.* **18**, 1397–1411 (2017).
22. M. Paillard *et al.*, MICU1 interacts with the D-ring of the MCU pore to control its Ca(2+) flux and sensitivity to Ru360. *Mol. Cell* **72**, 778–785.e3 (2018).
23. C. B. Phillips, C. W. Tsai, M. F. Tsai, The conserved aspartate ring of MCU mediates MICU1 binding and regulation in the mitochondrial calcium uniporter complex. *Elife* **8**, e41112 (2019).
24. M. Fan *et al.*, Structure and mechanism of the mitochondrial Ca(2+) uniporter holocomplex. *Nature* **582**, 129–133 (2020).
25. Y. Wang *et al.*, Structural insights into the Ca(2+)-dependent gating of the human mitochondrial calcium uniporter. *Elife* **9**, e60513 (2020).
26. C. Wang *et al.*, Structures reveal gatekeeping of the mitochondrial Ca(2+) uniporter by MICU1-MICU2. *Elife* **9**, e59991 (2020).
27. W. Zhuo *et al.*, Structure of intact human MCU supercomplex with the auxiliary MICU subunits. *Protein Cell* **12**, 220–229 (2021).
28. W. Wu *et al.*, The structure of the MICU1-MICU2 complex unveils the regulation of the mitochondrial calcium uniporter. *EMBO J.* **39**, e104285 (2020).
29. R. Payne, C. Li, J. K. Foskett, Variable assembly of EMRE and MCU creates functional channels with distinct gatekeeping profiles. *iScience* **23**, 101037 (2020).
30. T. E. Gunter, D. R. Pfeiffer, Mechanisms by which mitochondria transport calcium. *Am. J. Physiol.* **258**, C755–C786 (1990).
31. D. G. Nicholls, Mitochondria and calcium signaling. *Cell Calcium* **38**, 311–317 (2005).
32. P. Hess, J. B. Lansman, R. W. Tsien, Calcium channel selectivity for divalent and monovalent cations. Voltage and concentration dependence of single channel current in ventricular heart cells. *J. Gen. Physiol.* **88**, 293–319 (1986).
33. C. M. Armstrong, G. Cota, Calcium block of Na+ channels and its effect on closing rate. *Proc. Natl. Acad. Sci. U.S.A.* **96**, 4154–4157 (1999).
34. A. Azzi, E. Rossi, G. F. Azzone, Swelling and shrinkage phenomena in liver mitochondria. V. Permeability of the mitochondrial membrane to univalent cations: Effect of Mg++. *Enzymol. Biol. Clin. (Basel)* **7**, 25–37 (1966).
35. L. Packer, R. Utsumi, M. G. Mustafa, Oscillatory states of mitochondria. 1. Electron and energy transfer pathways. *Arch. Biochem. Biophys.* **117**, 381–393 (1966).
36. C. T. Settlement, G. R. Hunter, G. P. Brierley, Ion transport in heart mitochondria. 8. The effect of ethylenediaminetetraacetate on monovalent ion uptake. *Biochim. Biophys. Acta* **162**, 487–499 (1968).
37. J. P. Wehrle *et al.*, Mg2+ and the permeability of heart mitochondria to monovalent cations. *Arch. Biochem. Biophys.* **174**, 313–323 (1976).
38. G. P. Brierley, M. Jurkowitz, D. W. Jung, Osmotic swelling of heart mitochondria in acetate and chloride salts. Evidence for two pathways for cation uptake. *Arch. Biochem. Biophys.* **190**, 181–192 (1978).
39. P. Bernardi, A. Angrilli, G. F. Azzone, A gated pathway for electrophoretic Na+ fluxes in rat liver mitochondria. Regulation by surface Mg2+. *Eur. J. Biochem.* **188**, 91–97 (1990).
40. Y. Kirichok, G. Kravinsky, D. E. Clapham, The mitochondrial calcium uniporter is a highly selective ion channel. *Nature* **427**, 360–364 (2004).
41. A. Kapus *et al.*, Ruthenium red inhibits mitochondrial Na+ and K+ uniports induced by magnesium removal. *J. Biol. Chem.* **265**, 18063–18066 (1990).
42. V. Garg *et al.*, The mechanism of MICU-dependent gating of the mitochondrial Ca(2+) uniporter. *Elife* **10**, e69312 (2021).
43. B. D. Delgado, S. B. Long, Mechanisms of ion selectivity and throughput in the mitochondrial calcium uniporter. *Sci. Adv.* **8**, eade1516 (2022).
44. H. Vais *et al.*, EMRE is a matrix Ca(2+) sensor that governs gatekeeping of the mitochondrial Ca(2+) uniporter. *Cell Rep.* **14**, 403–410 (2016).
45. H. Vais *et al.*, Coupled transmembrane mechanisms control MCU-mediated mitochondrial Ca(2+) uptake. *Proc. Natl. Acad. Sci. U.S.A.* **117**, 21731–21739 (2020).
46. E. Berezhnaya, G. Hajnoczky, How do MICUs gate the mitochondrial calcium uniporter? *Cell Calcium* **100**, 102497 (2021).
47. J. J. Woods *et al.*, A selective and cell-permeable mitochondrial calcium uniporter (MCU) inhibitor preserves mitochondrial bioenergetics after hypoxia/reoxygenation injury. *ACS Cent. Sci.* **5**, 153–166 (2019).

48. R. G. Hansford, A. L. Lehninger, The effect of the coupled oxidation of substrate on the permeability of blowfly flight-muscle mitochondria to potassium and other cations. *Biochem. J.* **126**, 689–700 (1972).
49. A. Minta, R. Y. Tsien, Fluorescent indicators for cytosolic sodium. *J. Biol. Chem.* **264**, 19449–19457 (1989).
50. Y. Bernardinelli, G. Azarias, J. Y. Chatton, In situ fluorescence imaging of glutamate-evoked mitochondrial Na⁺ responses in astrocytes. *Glia* **54**, 460–470 (2006).
51. P. Donoso *et al.*, Fluorescence measurements of cytoplasmic and mitochondrial sodium concentration in rat ventricular myocytes. *J. Physiol.* **448**, 493–509 (1992).
52. D. O. Mak, W. W. Webb, Two classes of alamethicin transmembrane channels: Molecular models from single-channel properties. *Biophys. J.* **69**, 2323–2336 (1995).
53. A. N. Antony *et al.*, MICU1 regulation of mitochondrial Ca²⁺ uptake dictates survival and tissue regeneration. *Nat. Commun.* **7**, 10955 (2016).
54. M. Paillard *et al.*, Tissue-specific mitochondrial decoding of cytoplasmic Ca²⁺ signals is controlled by the stoichiometry of MICU1/2 and MCU. *Cell Rep.* **18**, 2291–2300 (2017).
55. R. Singh *et al.*, Uncontrolled mitochondrial calcium uptake underlies the pathogenesis of neurodegeneration in MICU1-deficient mice and patients. *Sci. Adv.* **8**, eabj4716 (2022).
56. J. C. Liu *et al.*, MICU1 serves as a molecular gatekeeper to prevent in vivo mitochondrial calcium overload. *Cell Rep.* **16**, 1561–1573 (2016).
57. V. Debattisti *et al.*, Dysregulation of mitochondrial Ca(2+) uptake and sarcolemma repair underlie muscle weakness and wasting in patients and mice lacking MICU1. *Cell Rep.* **29**, 1274–1286.e6 (2019).
58. N. Kohlschmidt *et al.*, Molecular pathophysiology of human MICU1-deficiency. *Neuropathol. Appl. Neurobiol.* **47**, 840–855 (2021).
59. V. Hung *et al.*, Proteomic mapping of the human mitochondrial intermembrane space in live cells via ratiometric APEX tagging. *Mol. Cell* **55**, 332–341 (2014).
60. T. König *et al.*, The m-AAA protease associated with neurodegeneration limits MCU activity in mitochondria. *Mol. Cell* **64**, 148–162 (2016).
61. Y. Wang *et al.*, Structural mechanism of EMRE-dependent gating of the human mitochondrial calcium uniporter. *Cell* **177**, 1252–1261.e13 (2019).
62. G. L. Decker, J. W. Greenawalt, Ultrastructural and biochemical studies of mitoplasts and outer membranes derived from French-pressed mitochondria. *Advances in mitochondrial subfractionation. J. Ultrastruct. Res.* **59**, 44–56 (1977).
63. C. W. Tsai *et al.*, Proteolytic control of the mitochondrial calcium uniporter complex. *Proc. Natl. Acad. Sci. U.S.A.* **114**, 4388–4393 (2017).
64. K. J. Kamer *et al.*, MICU1 imparts the mitochondrial uniporter with the ability to discriminate between Ca(2+) and Mn(2+). *Proc. Natl. Acad. Sci. U.S.A.* **115**, E7960–E7969 (2018).
65. N. E. Hoffman *et al.*, MICU1 motifs define mitochondrial calcium uniporter binding and activity. *Cell Rep.* **5**, 1576–1588 (2013).
66. C. W. Tsai *et al.*, Mechanisms and significance of tissue-specific MICU regulation of the mitochondrial calcium uniporter complex. *Mol. Cell* **82**, 3661–3676.e8 (2022).
67. G. Bhosale *et al.*, Pathological consequences of MICU1 mutations on mitochondrial calcium signalling and bioenergetics. *Biochim. Biophys. Acta Mol. Cell Res.* **1864**, 1009–1017 (2017).